Check for updates

Advanced Theory and Simulations

ADVANCED THEORY AND SIMULATIONS
www.advtheorysimul.com

RESEARCH ARTICLE OPEN ACCESS

Understanding Heavy and Light Hole Transport Dynamics in Diamond Through Monte Carlo Simulations and Experiments

Rina Yamazaki | Jan Isberg | Nattakarn Suntornwipat | Saman Majdi

Division of Electricity, Department of Electrical Engineering, Uppsala University, Uppsala, Sweden

Correspondence: Rina Yamazaki (rina.yamazaki@angstrom.uu.se)

Received: 21 November 2025 | **Revised:** 15 January 2026 | **Accepted:** 30 January 2026

Keywords: diamond | hole transport | monte carlo method | time-of-flight | wide bandgap semiconductors

ABSTRACT

Understanding the charge carrier properties and the effects of local scattering mechanisms in semiconductor materials is essential to realize reliable electronic devices. In this study, Monte Carlo simulations on hole transport in diamond were performed including multiple scattering mechanisms and the results are compared with experimental data observed by hole time-of-flight (ToF) measurements. By incorporating interband scattering, the deformation potential for acoustic phonon scattering was extracted. Furthermore, the redistribution of the heavy and light hole populations was recorded, and their dynamic behavior was analyzed. Moreover, detailed analysis uncovered distinct transport behaviors under complex scattering mechanisms, predominantly driven by optical phonon interactions, consistent with experimental observations.

1 | Introduction

Diamond has emerged as a highly promising semiconductor material because of its exceptional electronic and thermal properties. Its high carrier mobility, outstanding thermal conductivity, and large breakdown voltage enable reliable operation under extreme conditions, e.g. in high-power, high-temperature environments. These characteristics make diamond an attractive candidate for advanced power electronic applications [1]. Therefore, a detailed understanding of charge transport in diamond is not only of fundamental scientific interest, but also essential for the development of high-performance electronic devices.

The conduction band transport in diamond has been extensively investigated through both experimental and theoretical studies [2, 3]. Electrons in the six equivalent conduction band minima (valleys) exhibit transport behavior similar to that of holes under an applied electric field down to approximately 150 K. In this temperature range, the electron drift velocity increases linearly with electric field at low fields and saturates at higher fields. However, at temperatures below 150 K, the phenomenon of valley polarization emerges, leading to interesting transport characteristics. For instance, the occurrence of negative differential electron mobility in diamond has been reported [4, 5]. This phenomenon is attributed to intervalley scattering and electron–phonon interactions, with a maximum effect observed at 140 K. At temperatures below 100 K, intervalley scattering rates becomes negligible, leading to electron states with fixed valley polarization. The different responses of the electron effective masses along the longitudinal and transversal axes to the applied electric field give rise to two distinct transport modes corresponding to fast and slow electrons [6].

The valence band of diamond exhibits a markedly different structure compared to the conduction band. It contains three band maxima at the Γ point: the heavy-hole (HH), light-hole (LH), and split-off-hole (SO) bands with a small energy separation, 13 meV [7], relative to the HH and LH bands. Hole

This is an open access article under the terms of the Creative Commons Attribution License, which permits use, distribution and reproduction in any medium, provided the original work is properly cited.

© 2026 The Author(s). *Advanced Theory and Simulations* published by Wiley-VCH GmbH

transport involves interactions with phonons both within and between these bands. Although several experimental studies have investigated hole transport in diamond [4, 8, 9], the theoretical understanding remains comparatively limited. This issue is particularly important because boron, the most commonly used dopant in diamond, is an acceptor. As a result, the majority of bulk doped diamond-based electronic devices rely on the transport and control of holes.

In this study, hole transport in diamond was investigated in detail using the Monte Carlo method. Previous theoretical works have primarily focused on hole transport at low temperatures, considering only intraband acoustic (ac) and optical (op) phonon scattering within a single band (only HH was considered) [10]. In contrast, we extended the temperature range up to room temperature to examine how the dominant scattering mechanisms evolve with temperature. Also, both HH and LH bands were taken into account. Furthermore, interband ac phonon scattering was incorporated alongside intraband ac and op phonon scattering to obtain a more accurate determination of the deformation potential and to observe the behavior of holes between the bands. The simulation results were then compared with experimental data from time-of-flight (ToF) measurements. The ToF method is particularly well suited for probing intrinsic charge carrier transport, as it enables precise measurements of carrier velocity at very low carrier concentrations and in highly resistive materials. In this technique, electron–hole pairs can be generated by an external source, such as α-particles [11, 12] or a UV laser [13, 14], with the latter technique being employed in this study.

2 | Monte Carlo Method

The Monte Carlo method is a useful technique for understanding charge transport from theoretical perspectives. Electrical parameters obtained from measurements, such as deformation potentials, were incorporated into the simulation model to enable a detailed understanding of charge transport in semiconductor materials [15–19].

Diamond has three valence bands, and although the LH and SO bands are expected to contribute minimally due to their low density of states, including them (especially LH) is necessary for a more accurate simulation. Therefore, both HH and LH were incorporated into the simulation. In this study, the SO band is not included in the analysis. In diamond, the energy separation between the SO band and the HH/LH bands at the valence–band maximum is approximately 13 meV. As a result, the SO band can influence carrier transport, particularly at high temperatures or under strong electric fields. However, since this work aims to specifically investigate the interband scattering mechanisms between the HH and LH bands, only these two bands are considered in the model.

When the transport within the same band is considered (intraband), there are mainly two different scattering mechanisms: acoustic (ac) phonon scattering and optical (op) phonon scattering. When a hole interacts with ac phonons, it can gain or lose energy, which is called absorption and emission, respectively. The energy gained (emitted) by the scattering is assumed to be linearly related to the phonon energy as expressed below.

$$\epsilon = \hbar q \upsilon \tag{1}$$

Here, $\hbar$ is the reduced Planck constant, q is the magnitude of the phonon wave vector, and $\upsilon = 12.8$ km/s is the transverse phonon velocity.

The intraband ac phonon scattering rate is expressed as below [20].

$$P_{ac}(\vec{k'},\vec{k}) = \frac{q\pi D_{ac}^2}{4V\rho\upsilon}\left[1+3\cos^2(\vec{k'},\vec{k})\right]\left(\frac{1}{e^{\frac{\hbar q\upsilon}{k_BT}}-1}+\frac{1}{2}\mp\frac{1}{2}\right) \times\delta\left(E(\vec{k'})-E(\vec{k})\pm\hbar q\upsilon\right) \tag{2}$$

Here, $\vec{k}$ and $\vec{k'}$ are the initial and final hole wave vectors, D_{ac} is the ac phonon deformation potential, and $\rho = 3.51$ g/cm^3 is the density of diamond. The upper sign refers to absorption, and the lower sign refers to emission. This convention will be used throughout the paper. Because the hole gains or loses energy described in Equation (1), the energy of the hole after scattering can be written as follows.

$$E(\vec{k'}) = E(\vec{k}) \pm \hbar q \upsilon \tag{3}$$

$E(\vec{k})$ and $E(\vec{k'})$ are the initial and final hole energies. The final hole wave vector $\vec{k'}$ is affected by the phonon wave vector $\vec{q}$ and can be written as $\vec{k'} = \vec{k} \pm \vec{q}$. Under the approximation $k' \sim k$, the magnitude of the phonon wave vector can be expressed as $q = 2^{\frac{1}{2}}|k|^{\frac{1}{2}}(1-cos\Theta)^{\frac{1}{2}}$ where Θ is the angle between $\vec{k'}$ and $\vec{k}$. Therefore, by selecting the angle Θ at random, the phonon wave vector $\vec{q}$ is obtained. Then, the hole energy after the scattering event can be determined using Equation (3). Furthermore, since the valence band in diamond is strongly warped, the energy E can be written as

$$E(\vec{k}) = Ak^2 \mp \left[B^2k^2 + C^2k^2\left(sin^4\theta cos^2\psi sin^2\psi + sin^2\theta cos^2\theta\right)\right]^{\frac{1}{2}} \tag{4}$$

with $A = 2.670$, $B = 1.245$, $C = 1.898$ in units of $\frac{\hbar^2}{2m_0}$ where m_0 is the electron mass [21]. Here, θ and ψ are the polar and azimuthal angles of $\vec{k}$. The sign refers to HH and LH bands, respectively. This equation is used to determine $\vec{k'}$ through energy conservation, by equating it to the energy expression given in Equation (3).

In contrast, when a hole interacts with op phonons, it gains or loses a relatively higher and fixed amount of energy, approximately $\hbar\omega_{op}$ =167 meV. The scattering rate for intraband op phonon scattering can be written as follows [20].

$$P_{op}(\vec{k'},\vec{k}) = \frac{3\pi D_{op}^2}{2V\rho\omega_{op}a_0^2}\times\left(\frac{1}{e^{\frac{\hbar\omega_{op}}{k_BT}}-1}+\frac{1}{2}\mp\frac{1}{2}\right) \times\delta\left(E(\vec{k'})-E(\vec{k})\pm\hbar\omega_{op}\right) \tag{5}$$

Here, $D_{op} = 2.5\times10^9$ eV/cm is the op phonon deformation potential [10], $a_0 = 0.357$ nm is the lattice parameter. For op

25130390, 2026, 2, Downloaded from https://advanced.onlinelibrary.wiley.com/doi/10.1002/adts.202502259 by Rina Yamazaki - Uppsala University Library , Wiley Online Library on [09/03/2026]. See the Terms and Conditions (https://onlinelibrary.wiley.com/terms-and-conditions) on Wiley Online Library for rules of use; OA articles are governed by the applicable Creative Commons License

phonon scattering (emission) to occur, the hole energy has to exceed a threshold, which is, $E > \hbar\omega_{op}$. The energy of the hole after the op phonon scattering is;

$$E(\vec{k}') = E(\vec{k}) \pm \hbar\omega_{op} \tag{6}$$

Because both HH and LH bands are considered, holes interact not only within the same band but also between different bands. Interband ac phonon scattering most significantly affects the hole transport among all interband scattering mechanisms, and the corresponding scattering rate can be written as follows [22].

$$P_{ac}(\vec{k}', \vec{k}) = \frac{3q\pi D_{ac}^2}{4V\rho\upsilon} \sin^2(\vec{k}', \vec{k}) \left(\frac{1}{e^{\frac{\hbar q\upsilon}{k_B T}} - 1} + \frac{1}{2} \mp \frac{1}{2} \right) \times \delta\left(E(\vec{k}') - E(\vec{k}) \pm \hbar q\upsilon \right) \tag{7}$$

In our case, interband ac phonon scattering occurs through four processes: heavy to light (HH → LH) absorption and emission, and light to heavy (LH → HH) absorption and emission. Among them, the emission (HH → LH) scattering exhibits a threshold $E(\vec{k}) \geqslant 9.9 \times 10^{-4}$ eV [22]. The hole energy after the interband ac phonon scattering is expressed in the same way as in Equation (3).

In this work, the deformation potentials for both intraband and interband ac phonon scattering are assumed to be identical for the HH and LH bands, and the same assumption is made for op phonon scattering. This approximation is valid for hole states where the HH and LH bands remain close to the Γ point. In diamond, HH and LH states originate from the same fourfold-degenerate valence band maximum at the Γ point, and differences in their response arise from their distinct symmetry and effective masses rather than from different deformation potential values [23]. Accordingly, identical deformation potentials are used for the HH and LH bands.

Figure 1 shows the scattering rates for 80 and 300K, including all scattering mechanisms that we consider in the simulations. Overall, intraband and interband ac phonon scattering occur at any energy and can be the dominant scattering until the threshold of the intraband op phonon scattering (emission). As explained above, intraband op phonon scattering (emission) has a threshold. Therefore, the scattering rate is zero below this threshold, whereas it shows the highest scattering rate above it. Also, the difference between absorption and emission for ac phonon scattering is bigger in the HH than the LH band. With the same hole energy, the wave vector $\vec{k}$ in the HH band is larger than that in the LH band. This leads to a larger gap in the phonon number ($N_{ph} = \frac{1}{e^{\frac{\hbar q\upsilon}{k_B T}} - 1}$) between them, and can explain the difference between absorption and emission in HH and LH band [22]. While interband ac phonon scattering is stronger for light holes, other scattering mechanisms contribute more significantly to the total scattering of heavy holes. As a result, heavy holes dominate the overall transport process.

In our Monte Carlo simulation of hole transport in diamond, we modeled carrier dynamics in several steps to capture realistic transport behavior. Each cycle begins by selecting a drift time using a modified Newton's law of motion $\vec{\mathbf{F}} = \frac{\partial \hbar \vec{k}}{\partial t} = m_0 \vec{a}$, where $\vec{\mathbf{F}}$ is the force on the charged particle, and $\vec{\mathbf{a}}$ is the acceleration. The hole wave vector is then updated according to that drift interval, which triggers a recalculation of all momentum dependent scattering rates. A specific scattering event is chosen by the rejection technique [20], and after the event, the carrier's energy and momentum are updated. Repeating these steps produces a statistically robust picture of hole transport across varying conditions.

To update the hole energy after the scattering, Equation (3) is applied for intraband and interband ac phonon scattering, while Equation (6) is used for intraband op phonon scattering. Additionally, the momentum is updated by solving Equation (4) for the wave the $\vec{k}$, using the energy obtained from Equation (3) (for ac phonon scattering), or Equation (6) (for op phonon scattering) in accordance with the principle of energy conservation. This cycle is repeated until it satisfies certain conditions, such as the hole reaching the goal point or losing all the energy during transport.

To obtain ensemble-averaged transport quantities, each hole is simulated independently, and the process is repeated for 600 holes to obtain statistically reliable results. For each hole, the arrival time at the collecting electrode is recorded, with a maximum allowed time range between 0 and 80 ns, divided into 1000 bins. The contributions of all simulated holes are accumulated to obtain the transient current signal. The ToF is then extracted from current waveform by identifying the start time (t_{start}) and end time (t_{end}) of the current pulse. Finally, the drift velocity is calculated as

$$\upsilon_d = \frac{d}{t_{ToF}} \tag{8}$$

where d is the sample thickness and $t_{ToF} = t_{end} - t_{start}$ is the ToF.

3 | Time-of-Flight Measurement

To compare the simulation results with the experimental results, we conducted ToF measurement on a diamond sample. The diamond sample was grown by chemical vapor deposition (CVD) as electronic-grade material (Element Six Ltd.). It was measured 390 um in thickness and 5 × 5 mm in area, with an impurity concentration below 1×10^{13} cm^{-3}. Before the device fabrication, the sample was boiled in a graphite etch (HNO_3: H_2SO_4: $HClO_4$, 1: 1: 1) for 40 min at 180°C and oxygen-terminated in an oxygen plasma for 60 s to remove any surface contamination. A semitransparent mesh top contact (Ti/Al (15/200 nm)) was deposited by a Von Ardenne Magnetron Sputter on the sample to allow optical access and, at the same time, obtain a homogeneous electric field in the sample. Finally, the sample was mounted on a chip carrier.

The ToF technique has been used for the investigation of the charge transport properties in intrinsic materials such as diamond [3, 6, 24]. An illustration of the ToF setup is shown in Figure 2. In the system, free charge carriers are generated using a short light pulse (800 ps FWHM) from a quintupled Nd-YAG laser operating at a repetition frequency of 713 Hz and a wavelength of 213 nm, which corresponds to a photon

25130390, 2026, 2, Downloaded from https://advanced.onlinelibrary.wiley.com/doi/10.1002/adts.202502259 by Rina Yamazaki - Uppsala University Library , Wiley Online Library on [09/03/2026]. See the Terms and Conditions (https://onlinelibrary.wiley.com/terms-and-conditions) on Wiley Online Library for rules of use; OA articles are governed by the applicable Creative Commons License

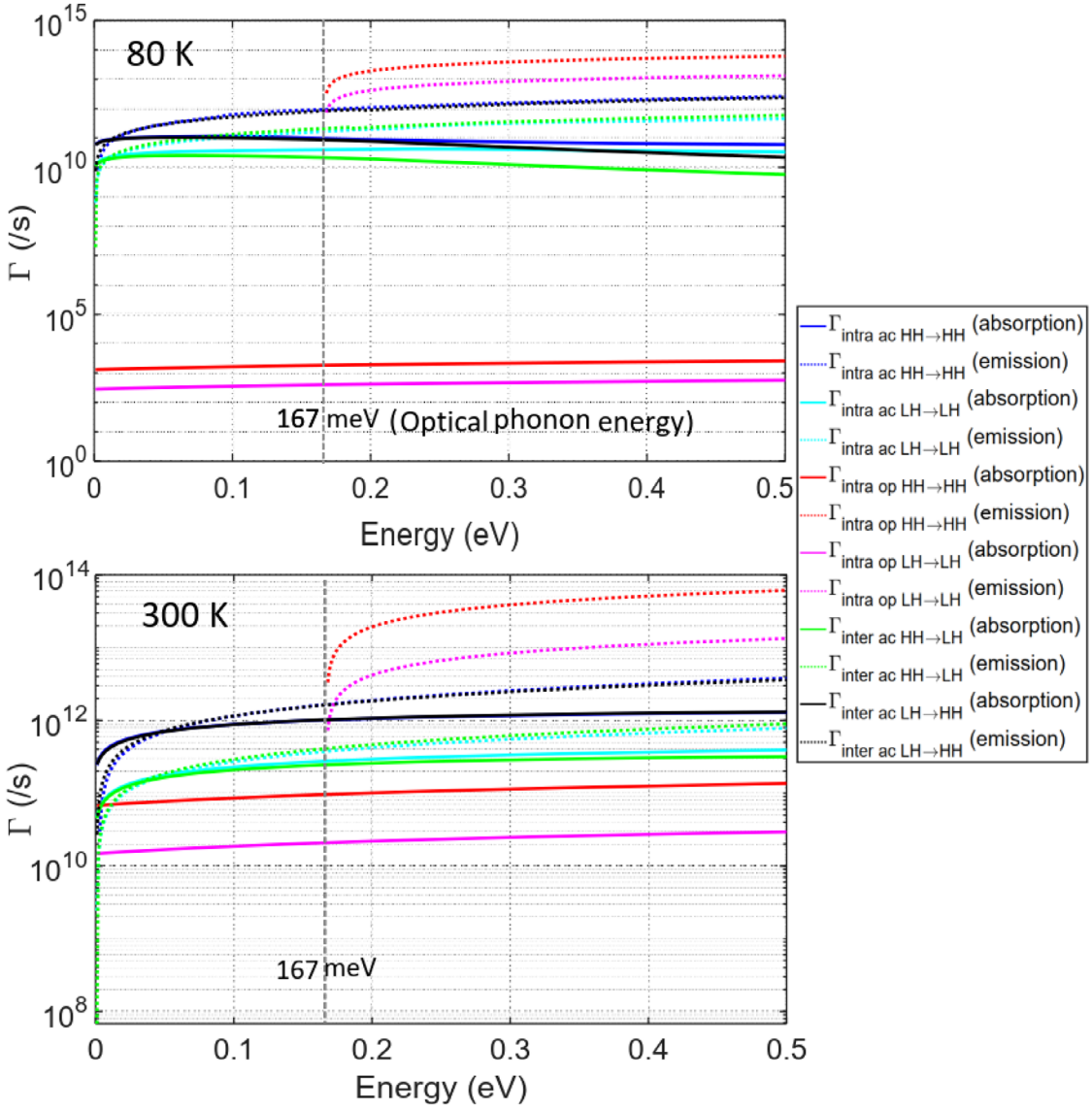

FIGURE 1 | Scattering rates of each scattering mechanism. The upper plot presents scattering rates at 80 K, while the lower plot shows results at 300 K. $D_{ac} = 10.10$ eV for ac phonon scattering, and $D_{op} = 2.45 \times 10^9$ eV/cm for op phonon scattering were used as the constants of the deformation potentials.

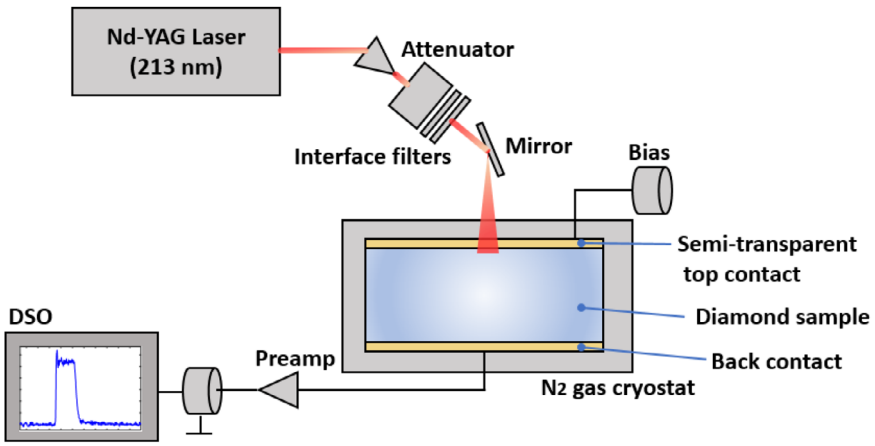

FIGURE 2 | Schematic illustration of the ToF setup using a 213 nm laser. The charge carriers are generated at the top contact within the sample near the top surface. Driven by the applied electric field, the carriers traverse the diamond substrate and are subsequently detected at the back contact.

25130390, 2026, 2, Downloaded from https://advanced.onlinelibrary.wiley.com/doi/10.1002/adts.202502259 by Rina Yamazaki - Uppsala University Library , Wiley Online Library on [09/03/2026]. See the Terms and Conditions (https://onlinelibrary.wiley.com/terms-and-conditions) on Wiley Online Library for rules of use; OA articles are governed by the applicable Creative Commons License

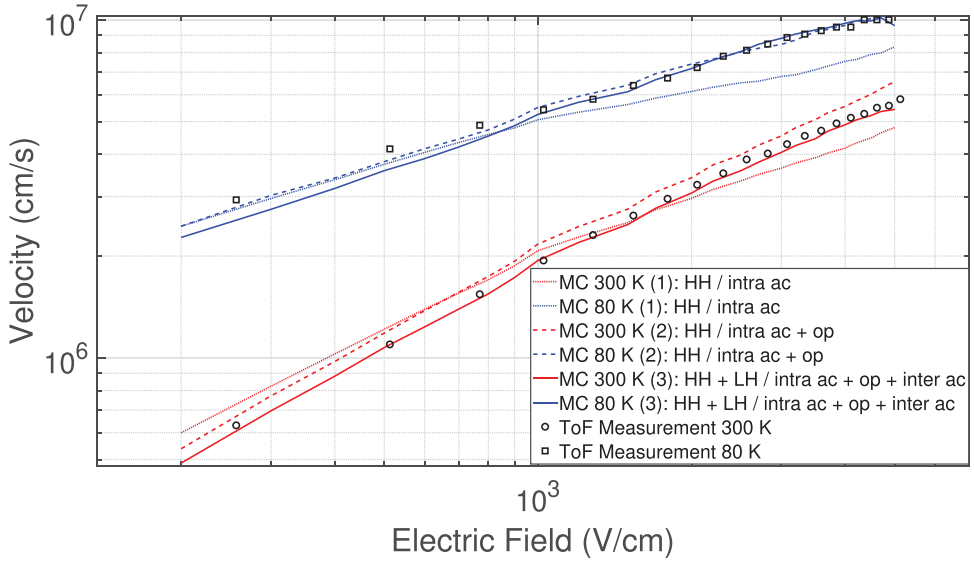

FIGURE 3 | Drift velocity results from Monte Carlo simulations are presented alongside ToF measurements. The ToF results are shown with circles, whereas simulation data are shown with red lines for 300 K and blue lines for 80 K. Three transport models were evaluated: (1) Single band (HH), only considering intraband ac phonon scattering and using a deformation potential of $D_{ac} = 9.00$ eV. (2) Single band (HH) model including both intraband ac and op phonon scattering, with D_{ac} as in (1), and $D_{op} = 2.45 \times 10^9$ eV/cm. (3) Two-band (HH and LH), with intraband ac, op, and interband ac phonon scattering, using $D_{ac} = 10.10$ eV and $D_{op} = 2.45 \times 10^9$ eV/cm.

energy of 5.82 eV. This energy is slightly above the diamond bandgap of 5.47 eV, resulting in an absorption depth of only a few micrometers and enabling highly localized excitation near the surface. Also, several interference filters were employed to block lower harmonics to ensure spectral purity, while neutral density filters were used to finely control the laser intensity. Because electron-hole pairs are generated close to the top contact, it becomes possible to observe the transport of either holes or electrons, depending on the applied bias polarity through the sample. The measured current at the back contact are amplified and displayed on an oscilloscope. A low-noise, broadband current amplifier with a 1 GHz bandwidth and 24 dB gain was used in conjunction with a digital storage oscilloscope (DSO) for the signal acquisition. The bias voltage was applied to the top contact as a 50 μs pulse using a bias-tee. This short pulsed bias enabled capacitive voltage distribution across the sample, and preventing undesirable charge accumulation. The diamond sample was wire-bonded onto a chip carrier and mounted in a Janis ST-100 vacuum cryostat with optical access, cooled using liquid nitrogen. A LakeShore 331 temperature controller, along with a calibrated TG-120-CU-HT-1.4H GaAlAs diode sensor in good thermal contact with the sample, was used for accurate temperature regulation. The measurement was done at the temperatures of 80 and 300 K with the applied voltage up to 200 V for the observation of the hole transport.

4 | Results and Discussion

Hole transport was simulated under three different scattering conditions: (1) considering a single band (HH), only with intraband acoustic (ac) phonon scattering, (2) a single band (HH) with both intraband ac and optical (op) phonon scattering, and (3) a two-band (HH and LH) with intraband ac and op phonon scattering, and interband ac phonon scattering. The op phonon scattering deformation potential $D_{op} = 2.45 \times 10^9$ eV/cm was used [10]. Also, the ac phonon deformation potential $D_{ac} = 9.00$ eV was used for simulation (1) and (2) [10], and $D_{ac} = 10.10$ eV was used for simulation (3). Different values were used between (1) and (2), and (3) because the best fit was shifted due to the introduction of the two-band and interband scattering. In addition, the extracted ac deformation potential is obtained under the assumption that the impurity does not significantly influence carrier transport. In reality, hole transport in diamond can also be affected by ionized and neutral impurity scattering. These mechanisms are not included in this model, and their contribution may therefore be partially reflected in the fitted deformation potential value. However, the impurity concentration in our samples is extremely low. Consequently, even if impurity scattering influences the effective deformation potential, its impact is expected to be negligible.

Simulations were performed at temperatures of 80 and 300 K, and the electric field from 0 to 5000 V/cm. The resulting drift velocity as a function of electric field is presented in Figure 3. The op phonon scattering involves higher energy exchange and therefore becomes the dominant scattering mechanism at higher electric fields. That is why simulation (1), which only involves intraband ac phonon scattering, shows a larger deviation from the experimental data at higher electric fields. Simulations (2) and (3) did not show a significant difference. From this, it was revealed that a single band with intraband ac and op phonon scattering (simulation (2)) is enough to simply simulate the velocity of the hole. However, by adding the LH band and interband ac phonon scattering (simulation (3)), a more precise deformation potential was obtained.

The scattering rates recorded during simulation (3) are plotted in Figures 4 and 5 for 80 and 300 K, respectively. The scattering rates in general are higher at 300 K due to the increased phonon

25130390, 2026, 2, Downloaded from https://advanced.onlinelibrary.wiley.com/doi/10.1002/adts.202502259 by Rina Yamazaki - Uppsala University Library , Wiley Online Library on [09/03/2026]. See the Terms and Conditions (https://onlinelibrary.wiley.com/terms-and-conditions) on Wiley Online Library for rules of use; OA articles are governed by the applicable Creative Commons License

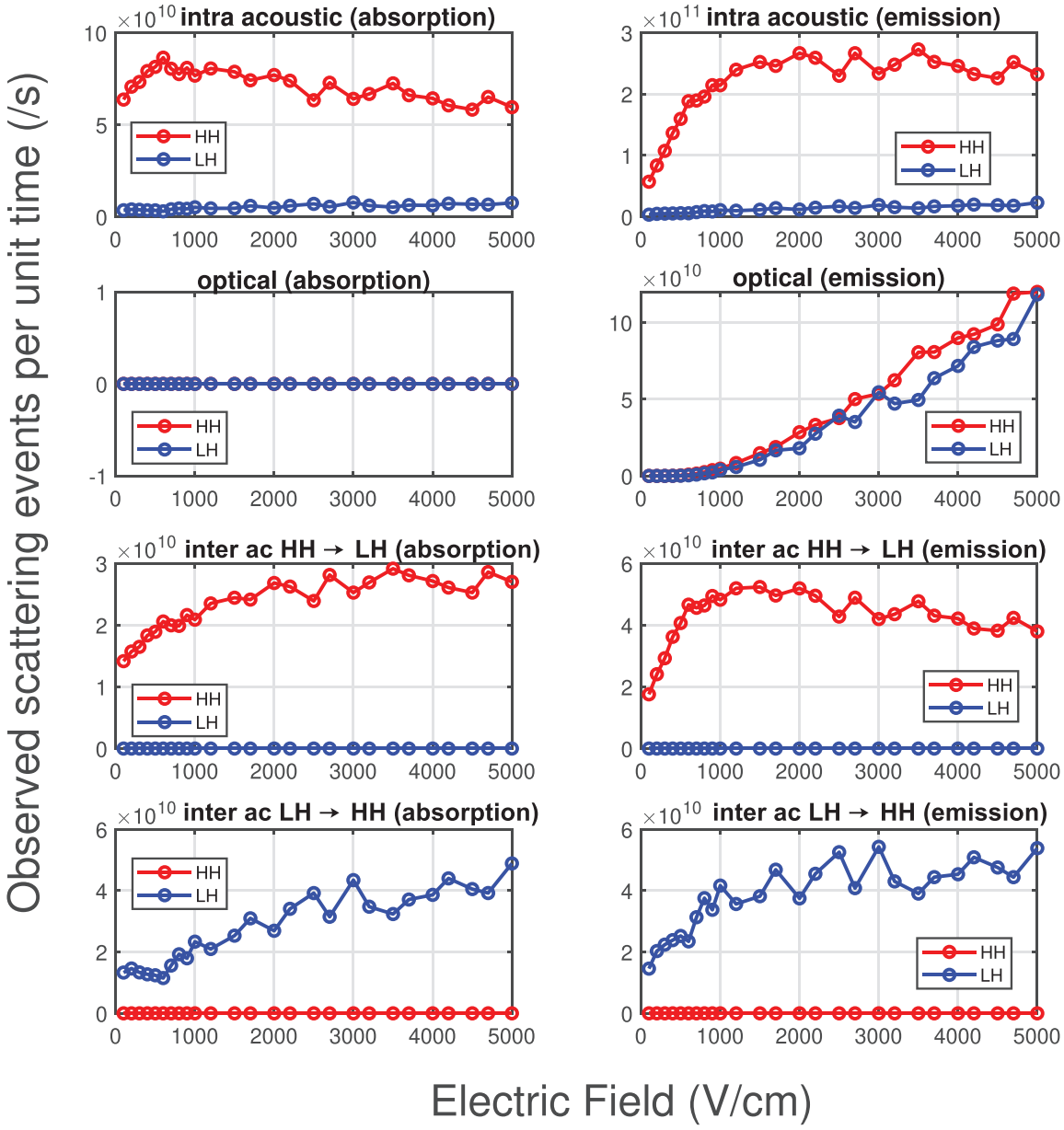

FIGURE 4 | The number of observed scattering events per unit time at 80 K obtained from simulation (3); red and blue lines indicate HH and LH, respectively.

occupation number (for example, $N_{ph} = 2.99 \times 10^{-11}$ at 80 K, and $N_{ph} = 1.56 \times 10^{-3}$ at 300 K), which leads to more frequent scattering in the diamond sample. Also, rates for heavy holes are higher than those of light holes, which shows the dominance of heavy holes in the transport. Intraband op phonon scattering (emission) increases with higher electric fields. As shown in Figure 1, it becomes the dominant scattering mechanism once the hole energy exceeds a certain threshold and acts to cool the holes, i.e. reduce their energy [10]. This energy loss through op phonon scattering contributes to a reduction in the number of other scattering events, such as ac phonon scattering. Consequently, the simulation results that include op phonon scattering show higher drift velocities compared to those with only ac phonon scattering. The op phonon scattering (absorption) is almost zero for 80 K, even though the scatterings were recorded for 300 K. This clearly reflects the assumption made in Figure 1. The behavior can be explained by the temperature dependence of the op phonon occupation number. Due to the relatively high op phonon energy in diamond, the phonon occupation number becomes extremely small at low temperatures. As a result, op phonon absorption processes, which are proportional to the phonon occupation number (Equation (5)), are strongly suppressed at 80 K, leading to a negligible intraband op phonon absorption scattering rate.

Figure 6 illustrates the extracted initial and final populations of the HH and LH bands, providing insight into their evolution. The initial states of the holes were subsequently determined using the weighting factors

$$w_{HH} = \frac{m_{HH}^{3/2}}{m_{HH}^{3/2} + m_{LH}^{3/2}} \text{ for HH, and } \quad w_{LH} = \frac{m_{LH}^{3/2}}{m_{HH}^{3/2} + m_{LH}^{3/2}} \text{ for LH} \tag{9}$$

25130390, 2026, 2, Downloaded from https://advanced.onlinelibrary.wiley.com/doi/10.1002/adts.202502259 by Rina Yamazaki - Uppsala University Library , Wiley Online Library on [09/03/2026]. See the Terms and Conditions (https://onlinelibrary.wiley.com/terms-and-conditions) on Wiley Online Library for rules of use; OA articles are governed by the applicable Creative Commons License

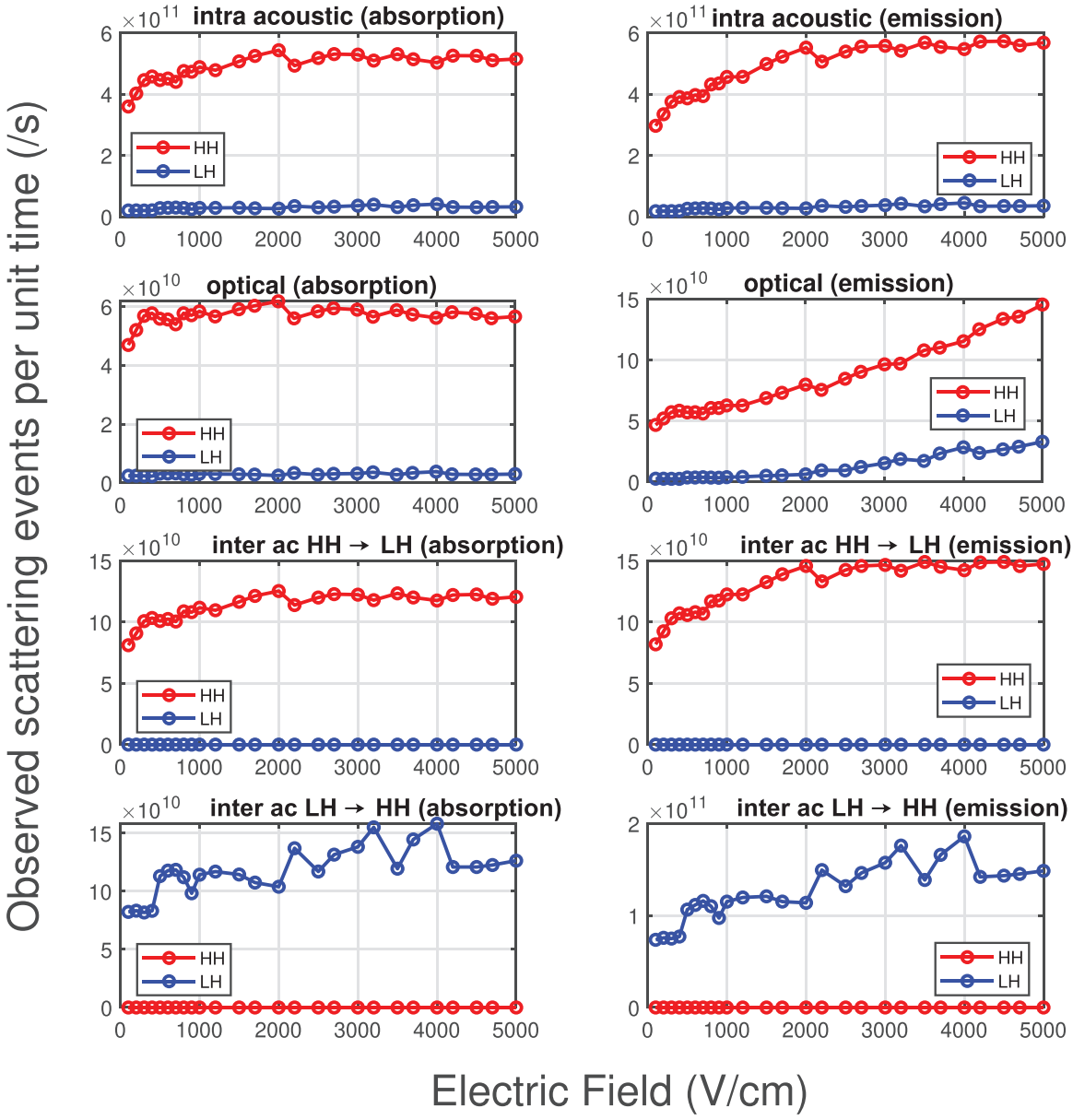

FIGURE 5 | The number of observed scattering events per unit time at 300 K obtained from simulation (3); red and blue lines indicate HH and LH, respectively.

which satisfy $w_{HH} + w_{LH} = 1$. Here, m_{HH} and m_{LH} are the effective masses of HH and LH, respectively. The simulation was performed for each hole and repeated for 600 holes. In each iteration, the initial state was assigned using a random function r ($0 \leq r \leq 1$). The hole was set to HH if $r < w_{HH}$ and to LH otherwise.

At 80 K, as the applied electric field increases, the final LH population becomes higher than the initial state, accompanied by a corresponding reduction in the final HH population, approximately 21 % at 5000 V/cm. At large wave vectors, the interband ac phonon scattering rate for HH → LH transitions exceeds that for LH → HH transitions. One contributing factor is the difference in effective masses between heavy and light holes ($m_{HH} = 0.667 \times m_0$, and $m_{LH} = 0.261 \times m_0$ for HH and LH, respectively [21]). Owing to their smaller effective mass, light holes can gain energy more rapidly from an applied electric field, which promotes intraband op phonon emission as the dominant relaxation mechanism (see Figure 1). This effectively reduces their excess energy, and consequently, interband ac phonon scattering from LH → HH becomes weaker. In contrast, heavy holes gain energy more slowly under the applied field, and therefore, experience only small changes in momentum, a regime in which interband ac phonon scattering (HH → LH) remains relatively strong. This enables efficient HH → LH transitions, while the reverse LH → HH process is suppressed at large momentum.

Additionally, at electric fields below 500 V/cm, a redistribution of the HH and LH populations is observed. This phenomenon may be attributed to the fact that, at low energies, the scattering rate for intraband and interband ac phonon scattering is higher for absorption than for emission, as shown in Figure 1. Consequently, LH carriers can more readily gain energy through

25130390, 2026, 2, Downloaded from https://advanced.onlinelibrary.wiley.com/doi/10.1002/adts.202502259 by Rina Yamazaki - Uppsala University Library , Wiley Online Library on [09/03/2026]. See the Terms and Conditions (https://onlinelibrary.wiley.com/terms-and-conditions) on Wiley Online Library for rules of use; OA articles are governed by the applicable Creative Commons License

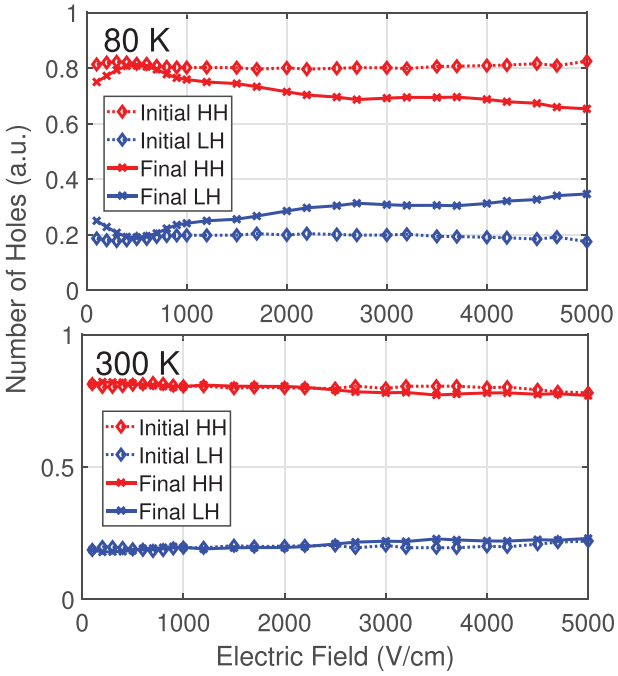

FIGURE 6 | The initial and final populations of HH and LH at 80 K (top figure) and 300 K (bottom figure). Red lines represent HH, while blue lines correspond to LH. Dot lines with indicate the initial populations, and solid lines denote the final populations.

phonon absorption compared to HH carriers, potentially leading to a redistribution behavior similar to that observed at higher electric fields.

The initial and final HH and LH populations exhibit only minor differences, at 300 K. This indicates that the thermal energy at this temperature is already sufficient to populate a broad range of states, so the hole distribution is close to equilibrium even before the electric field is applied. Consequently, the additional field induces only a marginal redistribution between the HH and LH bands.

Furthermore, the hole energy was recorded during simulation (3) and is presented in Figure 7. The top figure shows the simulation result of (1), the middle is of (2), and the bottom is of (3). Additional simulations in higher electric fields up to 10 kV/cm were performed to see the trend in the average energies. The figures of the simulation (1) and (2) show the stable average energy at the low electric field. The average energies are stable at around 9.9 and 9.9 meV at 80 K and 35.1 and 35.8 meV at 300 K for Simulation (1) and (2), respectively (at 10 V/cm). These values are close to the corresponding thermal energies of $\frac{3}{2}k_B T = 10.3$ meV and 37.9 meV at 80 and 300 K, respectively. This indicates that under the weak electric field, frequent ac phonon scattering maintains carriers close to thermal equilibrium. In Simulation (3), although the average energies at low electric field remain stable both for heavy and light holes, they are slightly lower than those obtained in Simulation (1) and (2) (approximately 8.9 and 8.6 meV at 80 K, and 33.8 and 33.3 meV at 300 K for HH and LH, respectively, under the electric field of 10 V/cm). This reduction is likely due to the energy exchange between HH and LH states induced by the interband ac phonon

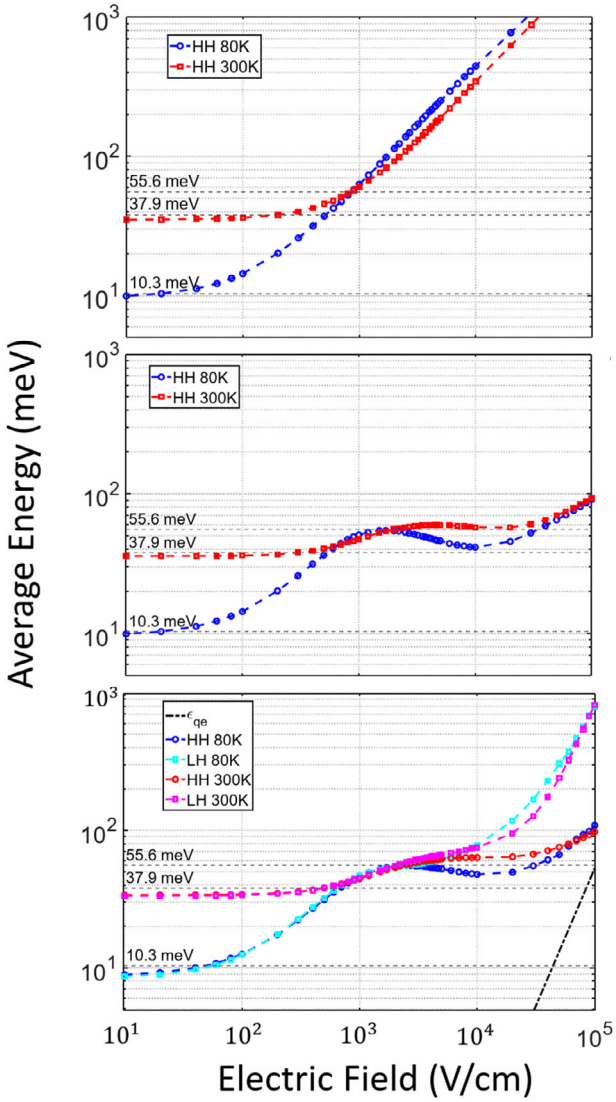

FIGURE 7 | Average energy of holes. The top figure is the result of the simulation (1) only with intraband ac phonon scattering, the middle is of the simulation (2) with intraband ac and op phonon scattering, and the bottom is of the simulation (3) with intraband ac, op, and interband ac phonon scattering. The dashed line in the bottom figure is the average energy with the quasielastic approximation (ϵ_{qe}). Reference lines show the thermal energy $\frac{3}{2}k_B T = 10.3$ meV at 80 K, $\frac{3}{2}k_B T = 37.9$ meV at 300 K, and the steaming motion approximation energy $\frac{1}{3}k_B\theta_{op} = 55.6$ meV.

scattering, which partially mitigates carrier heating by the electric field.

Moreover the average energies follow a certain trend [20], especially for simulations (2) and (3). In a low electric field, it is stable at the thermal energy: $< \epsilon >= \frac{3}{2}k_B T$. Around 2000 V/cm, the energy reaches that of the streaming motion approximation: $< \epsilon_{sm} >= \frac{1}{3}k_B\theta_{op} = 55.6$ meV, indicating that carrier heating becomes limited by op phonon emission. In a higher electric field, the energy starts following the trend of the energy of the quasielastic approximations [25]: $< \epsilon_{qe} >= \frac{3}{2}(k_B\theta_{op})\frac{E^2}{E_c^2}$, with E as the electric field, and E_C as a critical field. The critical field is expressed as $E_c = \frac{3^{3/2}m_h{}^2 D_{op}^2}{2^2\pi q\hbar^2\rho}$, with m_h as the effective

25130390, 2026, 2, Downloaded from https://advanced.onlinelibrary.wiley.com/doi/10.1002/adts.202502259 by Rina Yamazaki - Uppsala University Library , Wiley Online Library on [09/03/2026]. See the Terms and Conditions (https://onlinelibrary.wiley.com/terms-and-conditions) on Wiley Online Library for rules of use; OA articles are governed by the applicable Creative Commons License

mass of a hole, which corresponds to 2.18×10^5 V/cm in our case. In Figure 7, the slopes show good agreement with the trend of this energy approximation. The results confirm that op phonon scattering determines energy relaxation in the high-field regime. In addition, light holes begin to follow the quasielastic energy trend at lower electric fields, reflecting their more efficient acceleration. In contrast, heavy holes require substantially higher fields to reach the same regime, indicating that the larger HH effective mass delays the onset of transport dominated by op phonon scattering. This distinct behavior between HH and LH carriers is particularly pronounced in diamond, where the high op phonon energy enhances differences between carrier bands.

Another interesting observation is the energy drop of the heavy hole at 80 K above 2000 V/cm. As this phenomenon does not occur when only intraband ac scattering is considered (see the top figure in Figure 7 with simulation (1)), it is an effect of the op scattering. As seen in Figure 4, the op phonon scattering (emission) occurs at 80 K both for heavy and light holes, even though the absorption did not occur at all. This follows the assumption made in Figure 1. This means that, at high fields, relatively higher energy can be lost during transport (due to the op phonon scattering). Also, as seen from Equation (4), for the same energy loss, heavy holes have a greater effect than light holes in momentum that can be used for energy calculation, causing the big energy drop in the heavy hole at 80 K.

5 | Conclusions

Monte Carlo simulations were performed to study hole transport in diamond at 80 and 300 K under electric fields up to 5000 V/cm. Three modeling approaches were evaluated, progressively incorporating more scattering mechanisms. The simplest model, which included only intraband acoustic (ac) phonon scattering in the HH band, failed to reproduce the velocity trend observed in ToF measurements, particularly at high fields where optical (op) phonon scattering becomes dominant.

Adding op phonon scattering to the HH band significantly improved agreement with the experimental data. The most comprehensive model, which included both HH and LH bands along with intraband ac, op, and interband ac phonon scattering, provided the best match with measurements. This approach revealed distinct transport behaviors between heavy and light holes and allowed the extraction of a new ac deformation potential constant, $D_{ac} = 10.10$ eV. In addition, the population's redistribution of the HH and LH was observed in the simulation using the two-band structure, with the addition of interband ac phonon scattering.

These results highlight the HH and LH behavior in the transport, and the importance of including both op phonon and interband scattering mechanisms for accurate modeling of hole transport in diamond, especially under high electric fields. However, this methodology is not limited to diamond and can be broadly applied to characterize carrier transport in a wide range of semiconductor materials, offering a versatile framework for both theoretical and experimental investigations. In our model, several approximations are introduced in the calculation of scattering rates. In particular, for op phonon scattering, the hole states occupancy is assumed to remain sufficiently close to the Γ point. At elevated temperatures or under high electric fields, holes may populate regions farther from the Γ point, and under such conditions the present approximation may affect the quantitative accuracy of the results. Additionally, the model considers only the HH and LH bands. Incorporating the SO band would enable more precise simulations. Consequently, the current framework is best suited for providing qualitative insight and for use in regimes where these assumptions remain valid, rather than for a fully general description of hole transport.

Acknowledgments

The Swedish Energy Agency (Grant No. 48591-1) and the Swedish Research Council (Grant No. 04186-5) are gratefully acknowledged for financial support. In addition, Carl Tryggers Foundation (CTS 24:3542) is gratefully acknowledged by the authors.

Conflicts of Interest

The authors declare no conflicts of interest.

Data Availability Statement

Data supporting this study are available from the corresponding author upon reasonable request.

References

1. H. Umezawa, "Recent Advances in Diamond Power Semiconductor Devices," *Materials Science in Semiconductor Processing* 78 (2018): 147–156.

2. V. Djurberg, S. Majdi, N. Suntornwipat, and J. Isberg, "Determination of the Acoustic Phonon Deformation Potentials in Diamond," *Physical Review B* 106 (2022): 045205.

3. S. Majdi, M. Gabrysch, K. K. Kovi, N. Suntornwipat, I. Friel, and J. Isberg, "Low-Temperature Conduction-Band Transport in Diamond," *Applied Physics Letters* 109, no. 16 (2016): 162106.

4. A. Portier, F. Donatini, D. Dauvergne, M.-L. Gallin-Martel, and J. Pernot, "Carrier Mobility up to $10^6 cm^2 V^{-1} s^{-1}$ Measured in Single-Crystal Diamond by the Time-of-Flight Electron-Beam-Induced-Current Technique," *Physical Review Applied* 20 (2023): 024037.

5. J. Isberg, M. Gabrysch, S. Majdi, and D. J. Twitchen, "Negative Electron Mobility in Diamond," *Applied Physics Letters* 100, no. 17 (2012): 172103.

6. J. Isberg, M. Gabrysch, J. Hammersberg, S. Majdi, K. K. Kovi, and D. J. Twitchen, "Generation, Transport and Detection of Valley-Polarized Electrons in Diamond," *Nature Materials* 12, no. 8 (2013): 760–764.

7. M. Willatzen, M. Cardona, and N. E. Christensen, "Linear Muffin–Tin–Orbital and $k \cdot p$ Calculations of Effective Masses and Band Structure of Semiconducting Diamond," *Physical Review B* 50, no. 24 (1994): 18054–18059.

8. M. Gabrysch, S. Majdi, D. J. Twitchen, and J. Isberg, "Electron and Hole Drift Velocity in Chemical Vapor Deposition Diamond," *Journal of Applied Physics* 109, no. 6 (2011): 63719.

9. S. Majdi, V. Djurberg, N. Suntornwipat, M. Gabrysch, and J. Isberg, "Carrier Scattering Mechanisms: Identification via the Scaling Properties of the Boltzmann Transport Equation," *Advanced Theory and Simulations* 4, no. 1 (2021): 2000103.

10. S. Majdi, K. K. Kovi, J. Hammersberg, and J. Isberg, "Hole Transport in Single-Crystal Synthetic Diamond at Low Temperatures," *Applied Physics Letters* 102, no. 15 (2013): 152113.

11. H. Pernegger, S. Roe, P. Weilhammer, et al., "Charge-Carrier Properties in Synthetic Single-Crystal Diamond Measured with the Transient-Current Technique," *Journal of Applied Physics* 97, no. 7 (2005): 73704.

25130390, 2026, 2, Downloaded from https://advanced.onlinelibrary.wiley.com/doi/10.1002/adts.202502259 by Rina Yamazaki - Uppsala University Library , Wiley Online Library on [09/03/2026]. See the Terms and Conditions (https://onlinelibrary.wiley.com/terms-and-conditions) on Wiley Online Library for rules of use; OA articles are governed by the applicable Creative Commons License

12. S. Gkoumas, A. Lohstroh, and P. J. Sellin, "Low-Temperature Time-of-Flight Mobility Measurements on Synthetic Single-Crystal Diamond," *Diamond and Related Materials* 18, no. 11 (2009): 1338–1342.

13. C. Dorfer, D. Hits, L. Kasmi, et al., "Three-Dimensional Charge Transport Mapping by Two-Photon Absorption Edge Transient-Current Technique in Synthetic Single-Crystalline Diamond," *Applied Physics Letters* 114, no. 20 (2019): 203504.

14. Y. Oshiki, J. H. Kaneko, F. Fujita, et al., "Measurement of Charge Carrier Dynamics in Diamond Thin Films Using a Fast TOF System with a UV Pulsed Laser," *Diamond and Related Materials* 17, no. 4 (2008): 833–837.

15. L. Reggiani, C. Canali, F. Nava, and G. Ottaviani, "Hole Drift Velocity in Germanium," *Physical Review B* 16 (1977): 2781–2791.

16. M. Fischetti, "Monte Carlo Simulation of Transport in Technologically Significant Semiconductors of the Diamond and Zinc-Blende Structures. I. Homogeneous Transport," *IEEE Transactions on Electron Devices* 38, no. 3 (1991): 634–649.

17. F. M. Bufler, A. Schenk, and W. Fichtner, "Simplified Model for Inelastic Acoustic Phonon Scattering of Holes in Si and Ge," *Journal of Applied Physics* 90, no. 5 (2001): 2626–2628.

18. M. Costato, C. Jacoboni, and L. Reggiani, "Hole Transport in Polar Semiconductors," *Physica Status Solidi B* 52, no. 2 (1972): 461–473.

19. L. Reggiani, S. Bosi, C. Canali, F. Nava, and S. F. Kozlov, "Hole-Drift Velocity in Natural Diamond," *Physical Review B* 23 (1981): 3050–3057.

20. C. Jacoboni and L. Reggiani, "The Monte Carlo Method for the Solution of Charge Transport in Semiconductors with Applications to Covalent Materials," *Reviews of Modern Physics* 55, no. 3 (1983): 645–705.

21. N. Naka, K. Fukai, Y. Handa, and I. Akimoto, "Direct Measurement via Cyclotron Resonance of the Carrier Effective Masses in Pristine Diamond," *Physical Review B* 88, no. 3 (2013): 035205.

22. T. Brudevoll, T. A. Fjeldly, J. Baek, and M. S. Shur, "Scattering Rates for Holes Near the Valence-Band Edge in Semiconductors," *Journal of Applied Physics* 67, no. 12 (1990): 7373–7382.

23. G. L. Bir and G. E. Pikus, *Symmetry and Strain-Induced Effects in Semiconductors* (Wiley, 1974).

24. J. Isberg, S. Majdi, M. Gabrysch, I. Friel, and R. S. Balmer, "A Lateral Time-of-Flight System for Charge Transport Studies," *Diamond and Related Materials* 18, no. 9 (2009): 1163–1166.

25. L. Reggiani and M. Asche, *Hot-Electron Transport in Semiconductors*, Topics in Applied Physics, 1st edition, Vol. 58 (Springer Berlin Heidelberg, 1985).

25130390, 2026, 2, Downloaded from https://advanced.onlinelibrary.wiley.com/doi/10.1002/adts.202502259 by Rina Yamazaki - Uppsala University Library , Wiley Online Library on [09/03/2026]. See the Terms and Conditions (https://onlinelibrary.wiley.com/terms-and-conditions) on Wiley Online Library for rules of use; OA articles are governed by the applicable Creative Commons License